# NOTES

## Atmospheric Sounding Near 118 GHz

ALI D. S. ALI, PHILIP W. ROSENKRANZ AND DAVID H. STAELIN

*Research Laboratory of Electronics, Massachusetts Institute of Technology, Cambridge 02139*

21 February 1980 and 7 July 1980

ABSTRACT

The thermal emission spectrum of the atmosphere near the 118 GHz oxygen resonance has been measured from the NASA Convair-990 aircraft as it flew over clear air and storms. The instrument viewed the ground 45° from nadir with a 7.5° beamwidth. Brightness temperatures were measured in six bands 200 MHz wide centered at frequencies 821–1891 MHz from the line at 118.7505 GHz. The double-sideband super-heterodyne receiver had ~1 K sensitivity for 1 s integration. Comparison of observed clear air brightness temperatures (from 238 mb) with those computed for a coincident dropsonde yielded agreement within 1.4 K; the retrieved temperature profile agreed with the dropsonde with an average magnitude error of 1.4 K. Observations over precipitation yielded brightness perturbations as large as 30 K.

### 1. Introduction

In 1963, Meeks and Lilley (1963) proposed using the complex of oxygen ($O_2$) absorption lines at 60 GHz for temperature profile measurements. This technique was first successfully demonstrated in space by satellites launched in 1972 (Staelin *et al.*, 1973; Waters *et al.*, 1975), and in 1975 (Staelin *et al.*, 1977; Ledsham and Staelin, 1978).

Croom (1971) has discussed some of the advantages of the 118 GHz oxygen line relative to the 60 GHz complex for atmospheric probing: 1) It is an isolated line so that simpler superheterodyne radiometers may be used for sensing; 2) the $1^-$ line at 118.7505 GHz has the simplest Zeeman splitting pattern of all the $O_2$ lines, which is advantageous when retrieving temperature profiles at altitudes 50–150 km; and 3) for a given antenna diameter, the spatial resolution length at 118 GHz is half that for 60 GHz. Conversely, larger antennas are needed at 60 GHz for a given spatial resolution. The principal disadvantages of the 118 GHz line are the increased sensitivity to clouds (about twice that at 60 GHz), increased sensitivity to water vapor (about four times that at 60 GHz), and the slightly less advanced technology at 118 GHz.

This paper describes the first successful experiment for probing the atmosphere at 118 GHz. The first clear air temperature profile to be retrieved using this line is presented and compared with ground truth. This profile was probed by a downward viewing 6-channel radiometer, operated aboard the National Aeronautics and Space Administration (NASA) CV-990 aircraft flying near 238 mb. Ground truth was provided by a coincident dropsonde released from the CV-990.

Response of the radiometer system is also presented for rain cells viewed below the aircraft. Errors in the retrieved temperature profile caused by the raincells are presented and are consistent with raincell models.

### 2. The radiometer system

A double-sideband superheterodyne Dicke-switched spectrometer (Fig. 1) was operated aboard the NASA CV-990 aircraft for the NASA/NOAA (National Oceanic and Atmospheric Administration) Summer Microwave Hurricane Program (SMHP) during the summer and fall of 1978. The radiometer viewed 45° below the horizontal with a beamwidth of 7.5°. The local oscillator was centered precisely on the oxygen line frequency. The i.f. preamplifier for this system operated over the band 0.5–2.0 GHz and was followed by seven filter channels, each with a nominal bandwidth of 200 MHz, and one total power port; however, data from the most opaque channel (which is 607 MHz away from the center of the 118 GHz line) was rejected due to malfunctions. The fundamental integration time of the system was ~1 s, and the nominal rms sensitivity was 1 K.

Fig. 2 shows temperature weighting functions (looking down at ocean) for the six operating

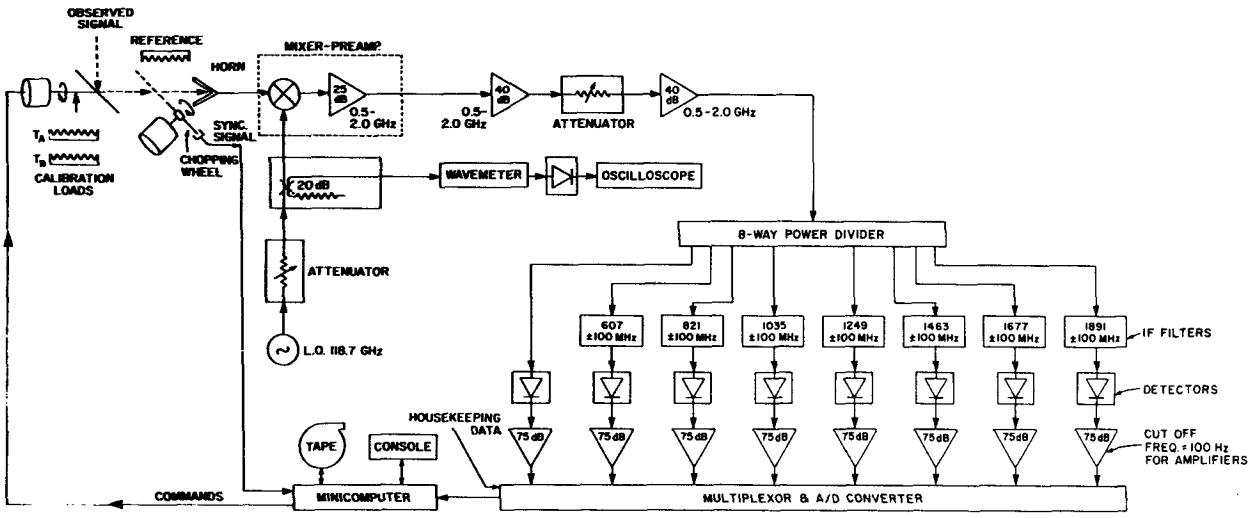


FIG. 1. Block diagram of the 118 GHz radiometer system.

filter channels. The weighting functions reveal the extent to which the brightness of each channel depends on kinetic temperature as a function of altitude (Meeks and Lilley, 1963). The absorption coefficients assumed for oxygen and water vapor were those of Liebe *et al.* (1977) and Waters (1976). In calculating these weighting functions, an exponential water vapor profile of 4 g $cm^{-2}$ and a scale height of 2 km was assumed. The sea surface was assumed to be a flat specular reflector.

### 3. Clear air observations and temperature profile retrievals

On 18 September 1978 (during SMHP flight 14) the radiometer looked down through clear atmosphere from an altitude of 33 000 ft and observed land near sea level and near 40°N, 122°W.

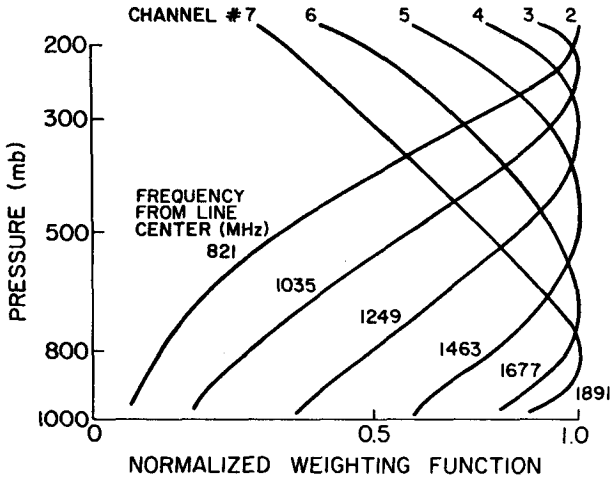


FIG. 2. Temperature weighting functions near 118 GHz for 45° view angle.

Brightness temperatures were calculated theoretically for radiosonde profiles obtained from stations in the vicinity of the aircraft, and extrapolated for comparison with the observed brightness temperatures. These extrapolations of 23 h and 2.5° latitude reduced the agreement between the observed and calculated brightness temperatures to only ~1–4 K, which is reassuring, but it does not permit high-quality retrievals.

During SMHP flight 17 on 7 October 1978, the NOAA group aboard the CV-990 released a dropsonde over the Pacific Ocean at 21°N, 109°W at 0108 GMT. The theoretical brightness temperatures for the dropsonde temperature and humidity profiles were compared to the brightness temperatures measured coincidentally by the radiometer at an altitude of 238 mb. Fig. 3 shows that the discrepancy between the observed and computed brightness temperatures is comparable to the radiometer sensitivity, ~1 K rms.

Brightness temperatures measured coincidentally with the dropsonde were inverted to retrieve the

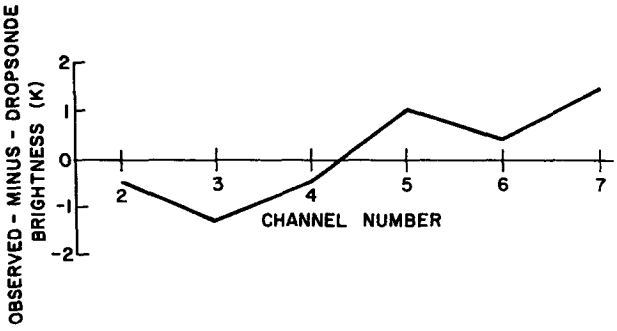


FIG. 3. Measured brightness temperatures less brightness temperatures theoretically calculated from coincident dropsonde data.

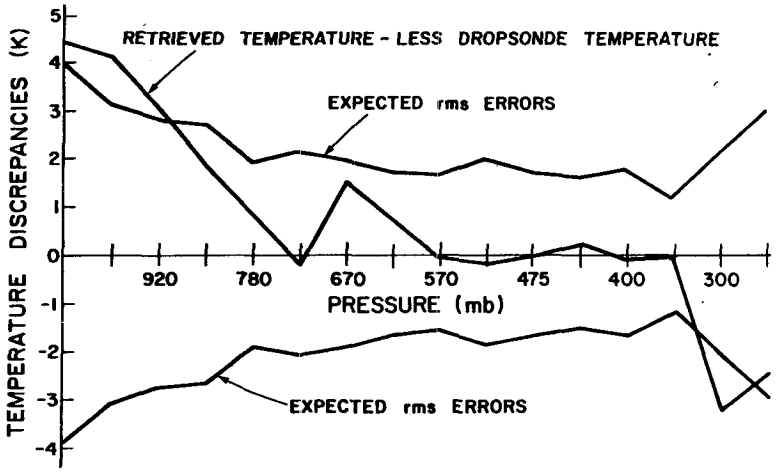


FIG. 4. rms residual errors (theoretical) and actual errors between estimated temperature profile and dropsonde measurement.

temperature profile. The inversion was done using the linear statistical approach, which is a multidimensional linear regression method. This method, discussed in detail by Rosenkranz *et al.* (1972), can be described briefly as follows. The vector of measured brightness temperatures $T_B$ is multiplied by a matrix **D** (not necessarily a square matrix), to yield the estimated temperature profile vector $\hat{\mathbf{T}}$, i.e.,

$$\hat{\mathbf{T}} = \mathbf{D}\mathbf{T}_B.$$

The matrix **D** was determined by minimizing the mean-square estimate error for a sample of 337 radiosonde records covering latitudes 30–60°S and 22–59°N. These radiosonde measurements were made January 1966–December 1968. The vector $\mathbf{T}_B$ includes a constant (unity) as one element.

Although the resulting rms error of the retrieved temperature profile is expected to be somewhat larger than necessary due to the wide span of latitudes and time employed in the *a priori* statistics, nonetheless it is much smaller than the *a priori* values. The absolute difference between the temperature profiles obtained from the 118 GHz data and the dropsonde is presented in Fig. 4 together with the expected rms errors; they are in good agreement. The two temperature profiles are plotted in Fig. 5. The largest error (~5 K) near the surface occurs over a range of altitudes much smaller than the resolution of any weighting function, and is consistent with the anticipated rms error.

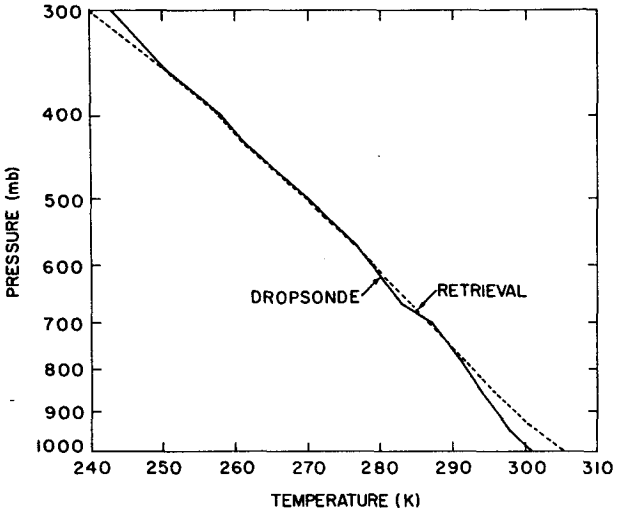


FIG. 5. Comparison of the retrieved temperature profile (using six channels) with the profile measured by a coincident dropsonde.

## 4. Raincell observations

Fig. 6 shows the response of channel 7 and channel 2 to two adjacent raincells probed by the system during SMHP flight 15. These channels are centered 1891 and 821 MHz, respectively, from the line center. Each point in Fig. 6 corresponds to ~1 s of integration time; gaps represent calibration periods. Fig. 7 presents five spectra observed at the times labeled A–D and R in Fig. 6. The spectra are shown as differences between the actual spectrum and the reference spectrum R obtained just prior to passage over the raincells.

Comparison of these microwave observations with theoretical calculations suggests that the rain-rate in these cells is $\geq 10$ mm h$^{-1}$. These calculations employed the rain absorption coefficients of Savage (1978), and were based on assumption of the Marshall-Palmer drop-size distribution, precipitation below the freezing level at ~810 mb,

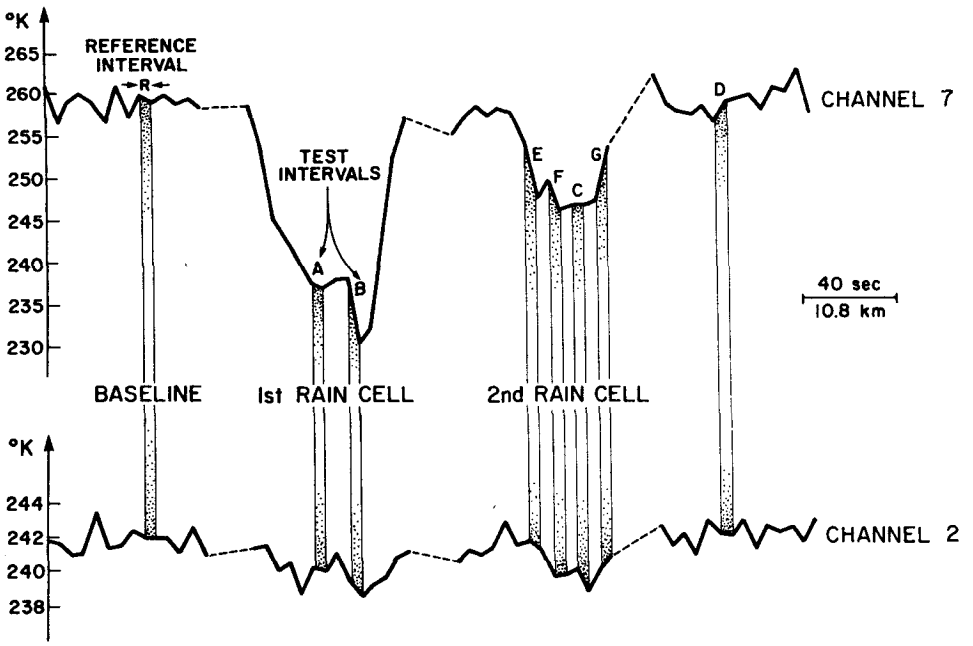


FIG. 6. Response of channels 2 and 7 to two adjacent raincells. Blank intervals are calibrations. Each point represents 1.2 s of integration time. Test intervals are discussed in text. Altitude = 29 000 ft; latitude: 49°58′–49°47′N; longitude: 184°17′–132°54′W.

and 60 mg cm$^{-3}$ clouds between ~500 and 850 mb. When temperature profiles are retrieved from this rain-perturbed data and compared to the temperature retrieval obtained just outside the rain cells, the errors listed in Table 1 result. The broken line in the table separates the cloudy part of the atmosphere (as observed visually from the airplane) from the clear air above the clouds. The large errors are confined to the cloudy part of the atmosphere. We have not attempted to correct the measurements for the effect of the rain or clouds because such a correction depends on the unknown cloud altitude and lapse rate beneath the cloud. In practice the best correction for such clouds

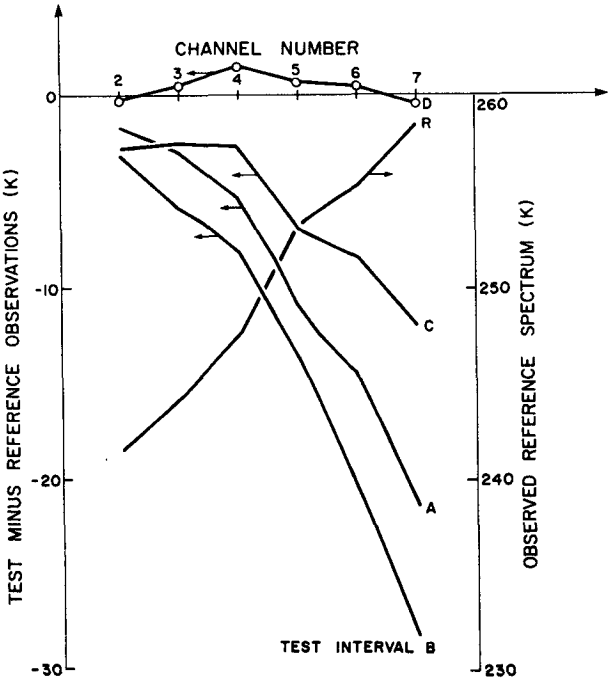


FIG. 7. Brightness temperatures of intervals indicated in Fig. 5 less the brightness temperature spectrum of the reference interval R. The curve labeled R is the reference spectrum.

TABLE 1. Raincell induced errors in the retrieved temperature profile (K). Dashed line marks cloud top.

| Pressure level (mb) | Interval E | F | C | G |
|---|---|---|---|---|
| 1000 | −18.9 | −19.7 | −18.7 | −10.7 |
| 950 | −17.2 | −18.0 | −17.2 | −8.0 |
| 920 | −16.0 | −16.9 | −16.1 | −7.5 |
| 850 | −13.3 | −14.1 | −13.6 | −6.3 |
| 780 | −9.9 | −10.8 | −10.7 | −5.0 |
| 700 | −5.6 | −6.5 | −6.8 | −3.2 |
| 670 | −5.1 | −6.1 | −6.4 | −3.0 |
| 620 | −4.4 | −5.3 | −5.7 | −2.7 |
| 570 | −3.5 | −4.5 | −4.9 | −3.3 |
| 500 | −2.1 | −3.1 | −3.7 | −1.8 |
| 475 | −1.3 | −2.3 | −3.0 | −1.4 |
| 430 | −0.3 | −1.2 | −2.2 | −1.4 |
| 400 | 1.4 | 0.2 | −0.7 | −0.3 |
| 350 | 2.3 | 1.2 | 0.3 | 0.1 |
| 315 | 3.2 | 2.2 | 1.2 | 0.7 |

will probably be to recognize and remove them, and then to interpolate cloud-free data to fill such new data gaps.

## 5. Conclusions

The observations of atmospheric emission near the 118 GHz resonance of oxygen agree well with theory in the spectral region 700–2000 MHz from the line center; the corresponding temperature profile retrievals are similarly satisfactory in the absence of heavy clouds or precipitation and are comparable to previous results near 60 GHz. Although these results are promising, more extensive comparisons would be desirable.

The principal effect of clouds is to cool the spectrum several degrees, particularly in the more transparent wings of the line. The spectrum responds primarily to an "effective altitude" for such clouds, which represents a combination of cloud density and altitude. Retrieval of more than one such cloud parameter would be relatively difficult. The discrete nature of the observed precipitation cells suggests that 118 GHz temperature profile maps of precipitating regions may often be quite satisfactory between these cells, and might be useful indicators of the size, location and perhaps intensity of the precipitation, provided the instrument spatial resolution is adequate.

Relative to the 60 GHz lines of oxygen, the principal advantages of 118 GHz are 1) twice the spatial resolution for a given antenna aperture, 2) simpler receiver design, 3) sensitivity to temperature somewhat higher in the mesosphere (at nadir), and 4) increased sensitivity (factor of ~2–3) to clouds and precipitation, for purposes of cloud retrievals. The principal disadvantages are 1) somewhat decreased receiver sensitivity for certain altitudes (which can be compensated by increased integration times), and 2) increased sensitivity of temperature retrievals to clouds, which is important primarily for high, heavy and extended clouds and precipitation that might not be identified and hence removed from temperature-retrieval maps (probably not too serious a problem).

*Acknowledgments*. We thank John W. Barrett and D. Cosmo Papa for their extensive help in the design and preparation of the instrument, David McDonough for providing much of the instrument software, Paul G. Steffes for the radio-frequency subsystems, Earl V. Peterson and George Alger for their assistance during the aircraft missions, and James C. Shiue for facilitating the program arrangements. The National Hurricane Center provided the radiosonde records, and NOAA supplied the dropsonde data. The project was supported by the National Aeronautics and Space Administration under Contract NAS5-23677, and the early stages of instrument development were funded under Air Force Contract F19628-75-C-0122.

## REFERENCES

Ali, A. D., 1979: 118-Gigahertz spectra of rain cells observed from aircraft. S.M. thesis, Dept. of Electrical Engineering and Computer Science, MIT, 114 pp.

Croom, D. L., 1971: The 2.53 mm molecular rotation line of atmospheric $O_2$. *Planet. Space Sci.*, **19**, 777–789.

Ledsham, W. H., and D. H. Staelin, 1978: An extended Kalman-Bucy filter for atmospheric temperature profile retrieval with a passive microwave sounder. *J. Appl. Meteor.*, **17**, 1023–1033.

Liebe, H. J., G. G. Gimmestad and J. D. Hopponen, 1977: Atmospheric oxygen microwave spectrum—experiment versus theory. *IEEE Trans. Antennas Propag.*, **AP-25**, 327–335.

Meeks, M. L., and A. E. Lilley, 1963: The microwave spectrum of oxygen in the earth's atmosphere. *J. Geophys. Res.*, **68**, 1683–1703.

Rosenkranz, P. W., F. T. Barath, J. C. Blinn, E. J. Johnston, W. B. Lenoir, D. H. Staelin and J. W. Waters, 1972: Microwave radiometer measurements of atmospheric temperature and water from an aircraft. *J. Geophys. Res.* **77**, 5833–5844.

Savage, R. C., 1978: The radiative properties of hydrometeors at microwave frequencies. *J. Appl. Meteor.*, **17**, 904–911.

Staelin, D. H., P. W. Rosenkranz, F. T. Barath, E. J. Johnston and J. W. Waters, 1977: Microwave spectroscopic imagery of the earth. *Science*, **197**, 991–993.

——, A. H. Barrett, J. W. Waters, F. T. Barath, E. J. Johnston, P. W. Rosenkranz, N. E. Gaut and W. B. Lenoir, 1973: Microwave spectrometer on the Nimbus 5 satellite: meteorological and geophysical data. *Science*, **182**, 1339–1341.

Waters, J. W., Absorption and emission by atmospheric gases, 1976: *Methods of Experimental Physics*, Vol. 12, *Astrophysics*, Part B, M. L. Meeks, Ed. Academic Press, 142–176.

——, K. F. Kunzi, R. L. Pettyjohn, R. K. L. Poon and D. H. Staelin, 1975: Remote sensing of atmospheric temperature profiles with the Nimbus 5 microwave spectrometer. *J. Atmos. Sci.*, **32**, 1953–1969.